Remote Sensing of Environment 314 (2024) 114408

Contents lists available at ScienceDirect

Remote Sensing of Environment

journal homepage: www.elsevier.com/locate/rse

Monitoring volcanic CO_2 flux by the remote sensing of vegetation on Mt. Etna, Italy

Nicole K. Guinn [a,*], Craig Glennie [a], Marco Liuzzo [b,c], Giovanni Giuffrida [d], Sergio Gurrieri [b]

[a] National Center for Airborne Laser Mapping, University of Houston, TX, USA
[b] Instituto Nazionale di Geofisica e Vulcanologia Sez, Palermo, Italy
[c] Dipartimento di Fisica e Scienze della Terra, Università di Ferrara, Ferrara, Italy
[d] Instituto Nazionale di Geofisica e Vulcanologia Sez, Catania, Italy

ARTICLE INFO

Edited by Jing M. Chen

Keywords:
Volcano monitoring
Soil CO_2 flux
NDVI
Mt. Etna
Remote sensing

ABSTRACT

Volcanic CO_2 is widely acknowledged as an important geochemical precursor for volcanic activity; however, obtaining observations through remote sensing remains a challenge. It is well established that volcanic CO_2 diffusely degases during magma ascent, and the volatiles interact with the ecosystem on the surface through CO_2 fertilization, which can improve vegetation health. A normalized difference vegetation index (NDVI) is a remote sensing method that quantifies vegetation health. This study compared NDVI signals from Landsat 8, MODIS, Sentinel 2, and VIIRS to soil CO_2 flux signals from 5 ground-based EtnaGas stations on Mt. Etna from 2011 to 2018. Due to variances in sensor and spectral characteristics, the NDVI values were calibrated across all 4 sensors. The 2nd derivatives of NDVI and soil CO_2 flux highlight the timeframes of the increase/decrease cycles of CO_2 degassing, which in turn, correspond to the change in storage levels as magma rises from an intermediate chamber to a shallow one. Between 2017 and 2018, the 2nd derivative spikes showed 16 magma recharge events in both NDVI and soil CO_2 signals. A flank analysis of homogenous trees across Mt. Etna showed the same 2nd derivative spike pattern for NDVI when compared to individual EtnaGas stations, indicating that trees do not have to be located within 30 m of volcano-tectonic structures to be affected by diffusely escaping volcanic CO_2. This study highlights the potential of NDVI as a remote sensing method for monitoring volcanic CO_2 emissions, paving the way for innovative approaches to volcanic surveillance.

1. Introduction

Carbon dioxide is the main exsolved magmatic volatile after water and increases in CO_2 flux can act as a precursor to eruptive activity; however, volcanic CO_2 is difficult to differentiate from atmospheric sources through remote sensing (Brantley and Koepenick, 1995; Burton et al., 2000; Symonds et al., 2001; Aiuppa et al., 2007; Liuzzo et al., 2013). Eruptions are triggered by magma moving towards the surface from depth, which releases volatiles as pressure decreases (Bottinga and Javoy, 1990; Brantley and Koepenick, 1995; Proussevitch and Sahagian, 1998; Burton et al., 2000; Gardner et al., 2000; Symonds et al., 2001; Aiuppa et al., 2007; Liuzzo et al., 2013). CO_2 is degassed earlier compared to other volatiles due to its low solubility in silicate melt and is commonly transported to the surface through faults, so it can serve as an early warning of volcanic activity (Farrar et al., 1995; Chiodini et al., 1998; Nuccio and Paonita, 2001; Liuzzo et al., 2015, 2021; Lewicki, 2021). Additionally, CO_2 degassing is often the only precursory event of deep magmatic intrusions since no or minimal deformation signals can be observed (Gurrieri et al., 2008; Liuzzo et al., 2013; Lewicki et al., 2019). Direct and continuous CO_2 measurement networks on volcanoes are valuable but are only present on ~2 % of the historically and persistently degassing, subaerial volcanoes (Burton et al., 2013; Schwandner et al., 2017; Aiuppa et al., 2019). Many volcanoes are not accessible for in-situ volatile measurements or for the installation of automatic sensors due to their remote location, hazards from volcanic activity, costly expenses, and/or political unrest (Houlié et al., 2006). Additionally, diffuse CO_2 emissions can be highly variable within several meters, so stationary, in-situ instruments are not able to depict this aspect (Fernández et al., 1998; Marín et al., 2005; Lewicki et al., 2017; Rahilly and Fischer, 2021). Because of this, CO_2 is poorly characterized for many volcanic systems, highlighting the need for alternative methods for CO_2 monitoring.

* Corresponding author at: 5000 Gulf Freeway, Houston, TX 77204, USA.
E-mail address: nkguinn@uh.edu (N.K. Guinn).

https://doi.org/10.1016/j.rse.2024.114408
Received 22 February 2024; Received in revised form 29 August 2024; Accepted 31 August 2024
Available online 4 September 2024

Many experiments have shown a positive correlation between photosynthesis and atmospheric CO_2 in both lab and natural settings (Drake et al., 1997; Curtis and Wang, 1998; LaDeau and Clark, 2001; Korner et al., 2005; Houlie et al., 2006; Cawse-Nicholson et al., 2018). The Free-Air Carbon dioxide Enrichment (FACE) studies were a series of short-term controlled CO_2 experiments on open ecosystems with the purpose of understanding how vegetation will react to rising atmospheric CO_2 levels (Ainsworth and Long, 2005; Cawse-Nicholson et al., 2018). Although FACE studies were short-term experiments, a meta-analysis of 3000 studies focused on plants growing in naturally CO_2 enriched areas demonstrated that FACE experiments also reasonably predict multigenerational plant responses with elevated CO_2 (Saban et al., 2019). Plant responses in volcanic and non-volcanic environments include increased photosynthesis and leaf starch but decreased stomatal conductance, leaf nitrogen content, and specific leaf area (Ainsworth and Long, 2005; Cawse-Nicholson et al., 2018; Saban et al., 2019). CO_2 fertilization from rising atmospheric levels accounts for 70 % of the current increase in global vegetation, or global greening (Saban et al., 2019). Vegetation greenness can be assessed through a remote sensing approach such as a normalized difference vegetation index (NDVI) which acts as a proxy for vegetation health (Cawse-Nicholson et al., 2018; Urbazaev et al., 2018). NDVI is calculated with respect to the near infrared (NIR) and red reflected values and ranges from 1 to 1. Typically, vegetation is recognized as NDVI 0.2, and healthy forests are NDVI 0.6 (Hashim et al., 2019).

Exsolved volcanic CO_2 escapes through the volcanic edifice at the summit or can seep into the soil on the volcano flanks and interact with the ecosystem on the surface (Allard et al., 1991; Symonds, 1998; Kern et al., 2017; Gurrieri et al., 2021). Trees that border faults or other high degassing areas are often naturally exposed to elevated CO_2 (Cook et al., 2001; Lewicki et al., 2014; Bogue et al., 2019). Many studies have noted that fluctuations of stable and unstable carbon isotopes as well as remote sensing analysis of a variety of vegetation types reflect volcanic diffuse degassing behavior (Pasquier-Cardin et al., 1999; Cook et al., 2001; Houlie et al., 2006; Evans et al., 2010; Lewicki et al., 2014; Seiler et al., 2017, 2021; Bogue et al., 2019). Coniferous forested areas of red firs and lodgepole pines on Mammoth Mountain, CA were killed in 1990 by excessive CO_2 concentrations in the soil that suffocated the roots of the trees (Farrar et al., 1995; Cook et al., 2001; Lewicki et al., 2007). Analysis of tree-ring isotopes such as ^{14}C showed that magmatic CO_2 on Mammoth Mountain was released through a crack in the impermeable layer covering a shallow volatile reservoir, formed by a magma intrusion rupture (Cook et al., 2001; Lewicki et al., 2014). Living trees on the margins of these kill zones were subjected to an additional 50 ppm of volcanic CO_2 (Cook et al., 2001). Over the next 15 years, unstable carbon isotopes indicated that these trees were exposed to an excess of 20 to 70 ppm with no visible signs of decreasing health (Lewicki et al., 2014). At Furnas caldera, Azores, 40 living plants in the temperate forests were assessed through ^{14}C and ^{13}C to determine an excessive exposure of 63 to 243 ppm from CO_2 degassing (Pasquier-Cardin et al., 1999). On Turrialba Volcano, Costa Rica, Bogue et al. (2019) found evidence of isotopically heavy ^{13}C in wood cores of two tropical plant species along a fault, indicating long-term photosynthetic incorporation of volcanic CO_2. In the Yellowstone caldera, NDVI analysis of the Tern Lake tree kill area indicated that the least healthy plants emphasized the central origin location of hydrothermal activity almost 15 years before previously determined with thermal and visual imagery (Bogue et al., 2023). Houlie et al. (2006) demonstrated that NDVI was elevated along a linear feature in a rift zone prior to a fissure eruption on Mt. Etna, Sicily, Italy. Through tree ring widths, Seiler et al. (2017) determined that vegetation growing nearby the fissure eruption on Mt. Etna was minimally affected by climate, precipitation, or the subsequent rise in soil temperature from the subsurface intrusion. However, based on inconsistent ^{14}C values in the tree rings (Seiler et al., 2021), it is still unknown if these vegetation enhancements were caused by the spatial variability in diffuse CO_2 degassing. Furthermore, Houlie et al. (2006) identified the enhanced NDVI two years before the eruption started, which is one of the earliest precursory signs and deserves further study to develop this volcanic monitoring technique. Other precursory signals include seismicity and deformation which earliest signs range from months or weeks before an eruption, whereas SO_2 flux and infrasound increases can be measured days to minutes before (Acocella et al., 2023).

These remote sensing and isotopes studies highlight that plants respond to diffuse, volcanic CO_2 degassing, often prior to eruptions or changes in volcanic activity, yet still contain many disadvantages. Tree kill areas are uncommon but emphasize the locations of harmful amounts of CO_2 being released through the soil. The isotopic studies involve in-situ field collections at discrete locations, which introduces many spatial and physical challenges in order to accurately characterize diffuse CO_2 degassing for a volcanic system. Additionally, the amount of excessive CO_2 that trees can tolerate before mortality varies greatly for coniferous, deciduous, and tropical trees (Pasquier-Cardin et al., 1999; Cook et al., 2001; Houlie et al., 2006; Evans et al., 2010; Lewicki et al., 2014; Seiler et al., 2017, 2021; Bogue et al., 2019), so further research is needed to understand how different types of trees will react to varying degrees of excessive volcanic CO_2. Furthermore, the current remote sensing studies of vegetation surviving in volcanic environments are incredibly limited in scope, focus on one or two species or dying trees, or lack a true, ground-truth connection to CO_2 flux. Volcanic CO_2 influencing plant health quantifiable by remote sensing has only been implied by process of elimination. Since minimal work focuses on the beneficial and high frequency impacts of volcanic CO_2 fertilization with trees, a high temporal resolution time series of CO_2 flux and satellite-derived tree health would highlight any direct and complex relationships, leading to the possibility of using trees as a proxy analysis for diffuse CO_2 degassing.

This study aims to characterize diffuse CO_2 degassing using NDVI. A significant portion of exsolved magmatic volatiles permeates through soil on the forested flanks of Mt. Etna (Allard et al., 1991; Symonds, 1998; Liuzzo et al., 2013). As volcanic activity fluctuates near a large population (Behncke and Neri, 2003; Burton et al., 2005; Allard et al., 2006; Aiuppa et al., 2007; Bonaccorso et al., 2011; Liuzzo et al., 2013), Mt. Etna has become one of the most robustly monitored volcanoes in the world (Bonaccorso et al., 2011; Paonita et al., 2021). Most notably, the EtnaGas network consists of 16 automatic stations that were functioning for all or a portion of the period between 01-01-2011 and 12-31-2018. All network stations continuously measure soil CO_2 flux, atmospheric temperature, atmospheric pressure, relative humidity, wind speed and direction, and active rainfall (Liuzzo et al., 2013). The stations were installed around Mt. Etna starting in 2002, close to volcano-tectonic structures previously characterized by strong diffuse CO_2 degassing emissions (Gurrieri et al., 2008; Liuzzo et al., 2013), several of which are located within homogenous forests on the upper flanks. The upper flanks contain both deciduous and coniferous trees, mainly European beech, Corsica black pine, downy oak, and holm oak (Seiler et al., 2017; Sciandrello et al., 2020). Homogenous forest in this case means a group of trees without bare ground or grass and not necessarily the same tree type. Over a ten-year period using the EtnaGas network, anomalous soil CO_2 flux measurements were observed prior to almost all volcanic activity (Liuzzo et al., 2013; Gurrieri et al., 2021; Paonita et al., 2021). Spaceborne estimates of NDVI for vegetation plus the multi-decadal time series of soil CO_2 flux on Mt. Etna provide a unique opportunity to develop a temporally continuous and spatially heterogenous model linking vegetation health and diffuse CO_2 emissions. If a correlation can be shown on Mt. Etna, then long-term monitoring of NDVI could be a tool to study CO_2 flux through a remote sensing approach on other vegetated as well as un-monitored volcanoes.

2. Methods

2.1. Soil CO_2 flux

Soil CO_2 flux measured by the EtnaGas stations were obtained from the Istituto Nazionale di Geofisica e Vulcanologia (INGV). The EtnaGas stations determine soil CO_2 flux through an empirical relationship that links the mole fraction of CO_2 obtained by mixing soil gas at 50 cm depth with air under controlled conditions (Gurrieri and Valenza, 1988) and soil permeability (Camarda et al., 2006a, 2006b; Liuzzo et al., 2013) by the equation:

$$_{CO_2} \quad 32 \quad 5\,8{*}k^{0\,24}\ {*}C_d \quad 6\,3{*}k^{0\,6}{*}C_d^3 \tag{1}$$

where $_{co_2}$ is the soil CO_2 flux expressed in kg m ^{2} d ^{1}, k is the numerical values of the gas permeability (35 m^2 for Mt. Etna), and C_d is the numerical values of molar fraction of the diluted CO_2 concentration. Hourly measurements were taken at every station at the top of each hour, but over the extended observation period, some stations experienced technical issues that resulted in occasional gaps in data, typically lasting no more than a few tens of days, due to sensor failures or environmental damage. During each soil CO_2 flux measurement, other environmental variables were collected such as atmospheric temperature and pressure, relative humidity, and active rainfall.

Using the same methods described in Liuzzo et al. (2013) and also described as follows, the soil CO_2 flux data for each EtnaGas station was reduced and filtered to aid interpretation and comparability (Appendix 3). The original hourly signal for each station was resampled to once a day by averaging the 24-h cycle and any missing days were filled in by linear interpolation. Moving averages were applied in order to remove periodic components shorter than a week. Additionally, moving averages were also applied to suppress seasonal components (300 to 400 days ^{1}). Any filtering applied to the soil CO_2 flux dataset was also applied to the corresponding coincident environmental observations.

2.2. Volcano-tectonic structures

Volcano-tectonic structures like faults and fissures are known to distribute exsolved volcanic CO_2, among other volatiles, from source to surface (Farrar et al., 1995; Chiodini et al., 1998; De Gregorio et al., 2002; Gurrieri et al., 2008; Liuzzo et al., 2013, 2021; Dietrich et al., 2016; Lewicki, 2021). The Mt. Etna flanks have 5 main fault systems: Pernicana Faults, Ripe della Naca Faults, Timpe Faults, South Faults, and Ragalna Faults (Barreca et al., 2013). These fault systems dominate the eastern and southern portions of the flanks, whereas the north and west are defined by a rift zone and eruptive fissures (Barreca et al., 2013; Liuzzo et al., 2013). Barreca et al. (2013) provided a GIS database of these volcano-tectonic structures in an effort to create a geographical and numerical representation of faults on Mt. Etna in a digital format (Fig. 1a).

Once emitted onto the surface through volcano-tectonic structures, diffuse volcanic CO_2 typically disseminates within a 10 to 30-m radius (Fernandez et al., 1998; Marín et al., 2005; Lewicki et al., 2017; Rahilly and Fischer, 2021; Bogue et al., 2023). All but one EtnaGas station on the flanks are located on or nearby a fault or fissure, so trees nearest the faults or fissures provided by Barreca et al. (2013) were assessed for their NDVI signal (Fig. 1b-f).

2.3. NDVI

NDVI is a dimensionless number that indicates photosynthetically active biomass and, therefore, vegetation health (Cawse-Nicholson et al., 2018), which can be seen in the visible spectrum as greenness. NDVI is calculated based on spectral reflectance using:

Table 1
The EtnaGas station names and locations based on the numbered labels in Fig. 1a.

Station #	Name	Latitude (N)	Longitude (E)
1	Maletto	37.793611	14.899722
2	Msm1	37.825833	14.983611
3	Albano	37.725278	14.942222
4	Brunek	37.808056	15.074167
5	Ripenaca	37.7625	15.0975
6	Passop	37.866944	15.045556
7	Roccacampana2	37.800278	15.136944
8	Fondachello	37.770556	15.216667
9	Primoti	37.701944	15.118889
10	SV1	37.696667	15.135278
11	P78	37.695278	15.143333
12	Parcoetna	37.630556	15.023056
13	3c	37.608611	15.082222
14	Agro	37.533611	14.898889
15	SML1	37.656944	14.920833
16	SML2	37.663611	14.905

$$NDVI \quad \frac{NIR \quad RED}{NIR \quad RED} \tag{2}$$

The near-infrared band (NIR) and red band (RED) are the reflected values determined by a radiometric sensor. When vegetation is healthy, there are larger amounts of chlorophyll and cell structures. Chlorophyll reflects green wavelengths and cell structures reflect near-infrared (NIR) wavelengths, while predominantly absorbing red wavelengths (Richardson and Wiegand, 1977; Kizilgeci et al., 2021). When plants are unhealthy, their cell structure breaks down resulting in more absorption of NIR wavelengths (Richardson and Wiegand, 1977; Kizilgeci et al., 2021); therefore, the more positive the NDVI number, the healthier the vegetation.

A variety of space-borne sensors and satellites were combined to create a relatively high temporal resolution NDVI signal using freely available and easily accessible data. Google Earth Engine (GEE; https://code.earthengine.google.com) was used as the search and data collection engine for NDVI. Between 2011 and 2018, there were 4 main satellite sensors that passed over Mt. Etna regularly: Landsat 8, Moderate Resolution Imaging Spectroradiometer (MODIS), Sentinel-2, and the Visible Infrared Imaging Radiometer Suite (VIIRS). Metadata for Landsat 8, MODIS, Sentinel-2, and VIIRS are expanded upon in Table 2. NDVI was calculated in GEE using Eq. (2) for Landsat 8 and Sentinel-2 after filtering all images for 0 % cloud cover between 2011 and 2018. MODIS and VIIRS had NDVI products already available on GEE; NDVI was also calculated using Eq. (2) but GEE also applied a 16-day best pixel threshold based on cloud cover. Any NDVI values under 0.4 were removed from all datasets to eliminate any effects from snow, deciduous trees losing their leaves in the winter, and a 16-day period of cloud cover. NDVI 0.4 is the typical value for moderate to dense forests with minimal to no bare ground (Laksono et al., 2020). Considering these 4 different sensors, no clouds, and averaging same day collections, this allowed for an average NDVI sampling frequency over the 2011 to 2018 time period of 7 3 days.

EtnaGas stations are located on the flanks of Mt. Etna at varying elevations, aspects, slopes, and ecosystems. The 5 highest EtnaGas stations (Brunek, Ripenaca, Msm1, Albano, and Maletto) are the only ones located within relatively homogenous forests and not near human influences such as agricultural fields, buildings, and roads (Fig. 1a). Brunek and Ripenaca EtnaGas stations are positioned almost on top of the Pernicana Fault System, Albano and Msm1 EtnaGas stations were installed near past eruptive fissures, and the Maletto EtnaGas station is not near any volcano-tectonic structures. Using these station locations as a geographical threshold, the NDVI was averaged either inside a 30-m buffer around a fault or averaged inside a polygon that encompassed only trees near an EtnaGas station (Fig. 1b-f). These polygons ranged in

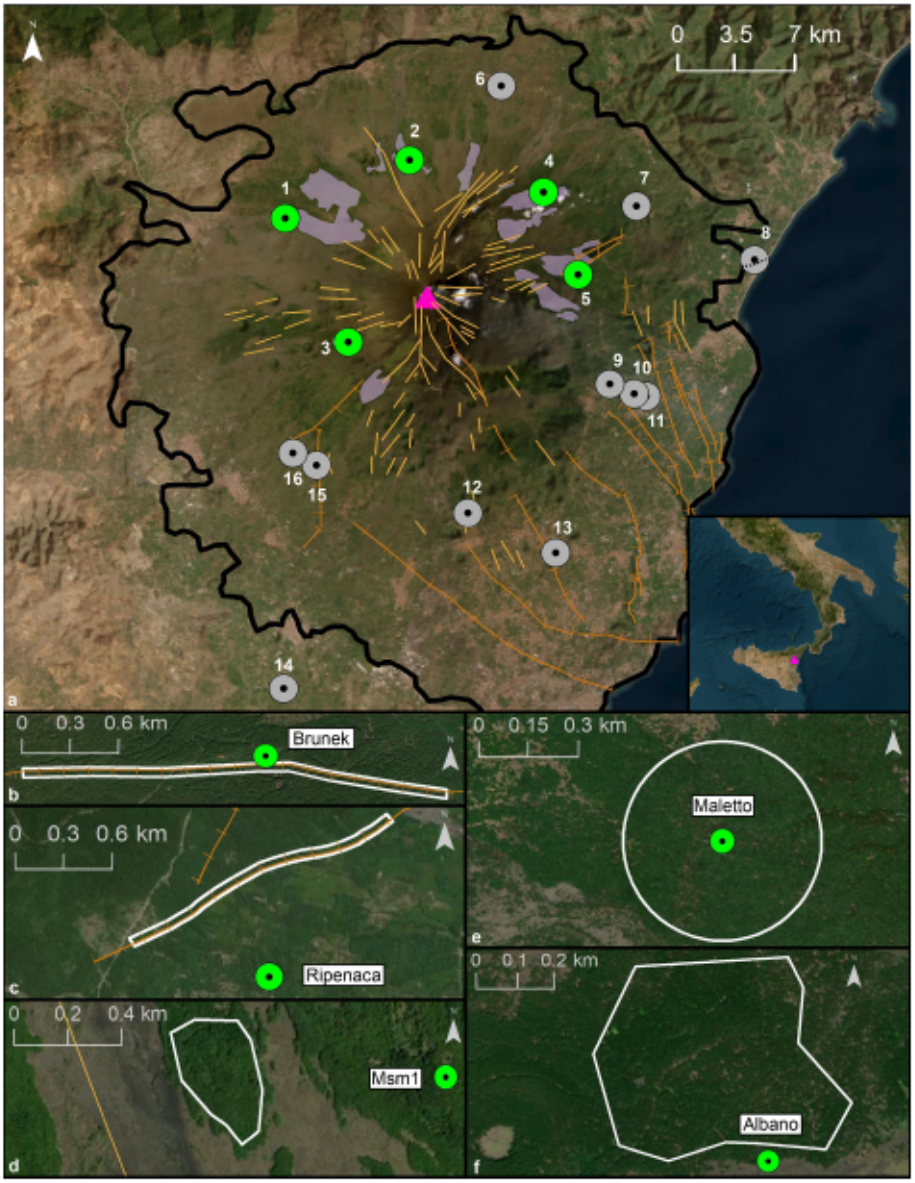

Fig. 1. a: A map of Mt. Etna with the EtnaGas stations as colored points (imagery: 46 cm resolution Maxar satellite photograph taken on 08-29-2022). Green colored stations are surrounded by homogenous forests and not near human influences, the other EtnaGas stations are shown in gray. Based on the numbered location, Table 1 expands on more EtnaGas station details. Yellow and orange lines are faults and eruptive fissures. Pink triangle delineates eruptive summit craters. Black outline is the Mt. Etna flank boundary. The purple polygons indicate where NDVI was averaged across the flanks of Mt. Etna. Inset map shows location of Mt. Etna within Italy and Sicily as a pink triangle. Figs. 1b through f illustrate the tree buffers around each station. 1b) 30 m buffer around the Pernicana Fault System, extending 1500 m east and west with the Brunek EtnaGas station as the center point. 1c) 30 m buffer along the Ripe della Naca Faults extending the closest 1500 m to the Ripenaca EtnaGas station. 1d) 99,000 m^2 area of trees between the Msm1 EtnaGas station and the closest eruptive fissure. 1e) 300 m buffer around the Maletto EtnaGas station to encompass only trees. 1f) 261,000 m^2 area encompassing only trees nearest the Albano EtnaGas station. Immediately south of Albano was a non-vegetated lava flow. (For interpretation of the references to colour in this figure legend, the reader is referred to the web version of this article.)

Table 2
Characteristics of Landsat 8, MODIS, Sentinel-2, and VIIRS.

Satellite/ sensor	GEE product	Spatial resolution	Date first available
Landsat 8	USGS Landsat 8 Collection 2 Tier 2 TOA Reflectance	30 m	2013-03-18
MODIS	MOD13Q1.061 Terra Vegetation Indices 16-Day Global 250 m	250 m	2000-02-18
Sentinel-2	Harmonized Sentinel-2 MSI: MultiSpectral Instrument, Level-2 A	10 m	2017-03-28
VIIRS	VNP13A1.002: VIIRS Vegetation Indices 16-Day 500 m	500 m	2012-01-17

size to comprise a wider range of trees when there was not a singular feature, like a fault, for diffusely escaping gas. Both MODIS and VIIRS have a large spatial resolution so whichever NDVI pixel overlapped with the buffer or polygon was collected.

2.3.1. Multi-sensor NDVI calibration

NDVI can be affected by different sensor and spectral characteristics such as sensor geometry, viewing angle, solar angle, atmospheric conditions, topography/radiometric/spatial resolution (Heinzel et al., 2006). Additionally, varying bandwidths for the red and NIR band also play a role (Heinzel et al., 2006). Furthermore, different footprint sizes across sensors include variability as land cover can change abruptly. An analysis of variance (ANOVA) test, which compares several sets of

observations simultaneously to analyze the difference between the means, confirmed that the mean NDVI values for Landsat 8, MODIS, Sentinel 2, and VIIRS are statistically different for 4 out of 5 EtnaGas stations at a 95 % confidence level (F_{score} $F_{critical}$). Therefore, to ensure consistent NDVI values across 4 different sensors, an inter-calibration technique was applied to the collected NDVI datasets at each EtnaGas station.

An iterative process following the methods of Heinzel et al. (2006) was conducted to remove cross-sensor relationships, minimize calculations, and to harmonize the datasets due to differences in spatial resolutions. Here, the methods completed for the Maletto EtnaGas station is described as an example, but the same processes were applied to all stations except the Ripenaca EtnaGas station, whose NDVI dataset passed the initial ANOVA test. All NDVI datasets for Landsat 8, MODIS, Sentinel 2, and VIIRS at the Maletto EtnaGas station were linearly interpolated to daily values, which had an original sampling frequency of 7 3 days. There was no extrapolation past the start dates and end dates of collection. Visually, MODIS and VIIRS NDVI timeseries appear to have similar values, while Landsat 8 and Sentinel 2 were generally lower or higher in comparison, respectively (Appendix 2). Considering this, the iterative process began by removing the qualifying regressions from Landsat 8 and Sentinel 2 with respect to MODIS or VIIRS until an ANOVA analysis proved the datasets were statistically the same. For the Maletto EtnaGas station to have comparable NDVI values across sensors, Landsat 8 was detrended with respect to VIIRS, and Sentinel 2 was detrended with respect to MODIS. Effects to Landsat 8 were quantified by subtracting VIIRS NDVI from Landsat 8 NDVI and plotting this difference with Landsat 8 NDVI to find the best fit line (Appendix 2, Table 3). The best fit line was a 2nd order polynomial with an r^2 0.5, and this relationship was removed from the Landsat 8 NDVI. The removal of outliers (3) resulted in an almost identical best fit line and considered unnecessary. The same process was completed to remove effects from Sentinel 2 with respect to MODIS (Appendix 2, Table 3). Similar, non-linear results were also collected by Heinzel et al. (2006) using Landsat 5, QuickBird, ASTER, and SPOT 5.

Msm1, Albano, and Brunek EtnaGas stations also had visually similar NDVI graphs as the Maletto EtnaGas station (Appendix 2). Generally, for these remaining EtnaGas stations, Landsat 8 and Sentinel 2 NDVI were detrended through 2nd order polynomials with respect to MODIS or VIIRS in order to have consistent estimates across all sensors. Table 3 shows all the 2nd order polynomial equations removed at each station. At the Albano EtnaGas station, Landsat 8 was detrended with respect to VIIRS, Sentinel 2 was detrended with respect to MODIS, and VIIRS was detrended with respect to MODIS. At the Brunek EtnaGas station, Landsat 8 was detrended with respect to MODIS. At the Msm1 EtnaGas station, Landsat 8 was detrended with respect to MODIS, and Sentinel 2 was detrended with respect to MODIS. The Ripenaca EtnaGas station did not need any changes since the ANOVA analysis confirmed statistically similar means with the original NDVI data. In summary, for all stations except for Ripenaca, Landsat 8 and Sentinel 2 were recalibrated with the addition of recalibrating VIIRS at the Albano EtnaGas station. The NDVI values calculated in this section will be referred to as calibrated NDVI.

Table 3
The best fit regressions for each EtnaGas station. These are the equations that resulted in an ANOVA test of F_{score} $F_{critical}$ at 95 % confidence level to have statistically the same means. Using Maletto 1st column, 1st row as an example, the x values are the Landsat 8 NDVI. The y values are the difference between Landsat 8 and VIIRS NDVI. The y values are subtracted from the x values to remove the relationship.

EtnaGas Station	Landsat 8 NDVI w.r.t VIIRS NDVI	Landsat 8 NDVI w.r.t MODIS NDVI	Sentinel 2 NDVI w.r.t MODIS NDVI	VIIRS NDVI w.r.t. MODIS NDVI
Maletto	y 7.58 ^{2} 11.2 -4.19		y 0.03 ^{2} 1.07 -0.9	
Albano	y 2.3 ^{2} 2.13 0.41		y 1.22 ^{2} 2.51 -1.12	y 0.42 ^{2} 0.2 -0.08
Brunek		y 0.41 ^{2} 1.81 -1.08		
Msm1		y 2.62 ^{2} 3.32 1.03	y 1.45 ^{2} 1.84 0.67	

2.4. Filtering

Diffuse degassing is typically concentrated at volcano-tectonic structures, where it is facilitated by higher permeability in the fault areas. Nevertheless, it is possible that diffuse degassing is present throughout the entire volcanic structure, with its intensity fluctuating based on soil permeability levels. Due to potential volcanic CO_2 influence at all areas on the flanks, environmental parameters were used to filter out external influences from the calibrated NDVI and soil CO_2 flux signals instead of using a control group of trees far away from volcano-tectonic structures but still on the flanks. In addition, the environmental parameters (atmospheric temperature and pressure, relative humidity, and active rainfall) can influence both NDVI and soil CO_2 flux measurements and were filtered out to minimize any effects (Curtis and Wang, 1998; LaDeau and Clark, 2001; Korner et al., 2005; Liuzzo et al., 2013; Seiler et al., 2017).

Soil moisture impacts soil degassing and is strongly related to the relative humidity parameter (Liuzzo et al., 2013); however, the impact has a short timescale. The resampling of the soil CO_2 flux data in section 2.2 which filtered frequencies less than a week removes relative humidity effects (Liuzzo et al., 2013). The relatively longer temporal resolution of the calibrated NDVI signals in section 2.3.1 consequentially did not have any effects from relative humidity. Indeed, a linear regression analysis between the calibrated NDVI and soil CO_2 flux signals with relative humidity for each station shows no relationship (Table 4). Maletto and Albano were missing relative humidity measurements, but their soil CO_2 flux was considered to not be impacted by humidity due to the negligible pattern at the other 3 stations. These results agree with the similarly resampled soil CO_2 flux of the EtnaGas stations in Liuzzo et al. (2013) for the 2002 2012 timeframe, that all had no trends with respect to relative humidity.

All other environmental variables that affected the calibrated NDVI and soil CO_2 flux signals were removed based on a linear regression analysis (Table 4). The environmental factors were resampled to the same collection dates as the calibrated NDVI signals, whereas the resampled soil CO_2 flux data and corresponding environmental constituents from section 2.2 were used for the linear regression analysis. The calibrated NDVI signal along the Pernicana fault nearby the Ripenaca EtnaGas station and the soil CO_2 flux signal at the Brunek EtnaGas station were most affected by temperature. Atmospheric pressure and rainfall did not show significant correlation to the calibrated NDVI or soil CO_2 flux signals. The temperature linear regression was removed from the impacted signal when r^2 0.1 to minimize even the weakest external effects. Maletto and Albano EtnaGas stations were missing rainfall measurements but were presumed to not be influenced since the other stations had a maximum r^2 of 0.03. Additionally, vegetation in Mediterranean climates is influenced more by air temperature than by precipitation (Seiler et al., 2017), and plants are accustomed to the high permeability of volcanic soil which limits surface runoff (Houlie et al., 2006). Therefore, droughts or excessive precipitation do not significantly impact the vegetation on Mt. Etna on short time scales.

In previous studies, the 2011 2019 soil CO_2 flux data from the EtnaGas stations were filtered through methods developed by the Observatoire Volcanologique du Piton de la Fournaise (OVPF) and by a moving average filter (MAFILT) (Gurrieri et al., 2021). However, this study opted for filtering based on linear regression analysis since the soil CO_2 flux was compared to the NDVI signal, which was at a much lower temporal resolution. Consistent filtering for both NDVI signals and soil

Table 4
The r^2 values of the linear regression analysis between an environmental parameter and the calibrated NDVI and soil CO_2 flux of an EtnaGas station. T = temperature, P = pressure, rH = relative humidity, and Pr = precipitation/active rainfall.

EtnaGas station	Calibrated NDVI				Soil CO_2 flux			
	T	P	rH	Pr	T	P	rH	Pr
Ripenaca	0.6	0.09	0.04	0.02	0.2	0.05	0.002	0.003
Brunek	0.2	0.03	0.002	0.03	0.5	0.001	0.007	0.005
Maletto	0.12	0.03	N/A	N/A	0.02	0.007	N/A	N/A
Msm1	0.4	0.000	0.0009	0.0008	0.1	0.02	0.002	0.001
Albano	0.12	0.05	N/A	N/A	0.09	0.003	N/A	N/A

CO_2 flux signals minimize the change of introducing biases or aliasing into one of the signals. The visual effects of filtering on the time series are in Appendix 2.

3. Data & Discussion

3.1. Quantitative

To better compare data across the Mt. Etna flanks, the calibrated

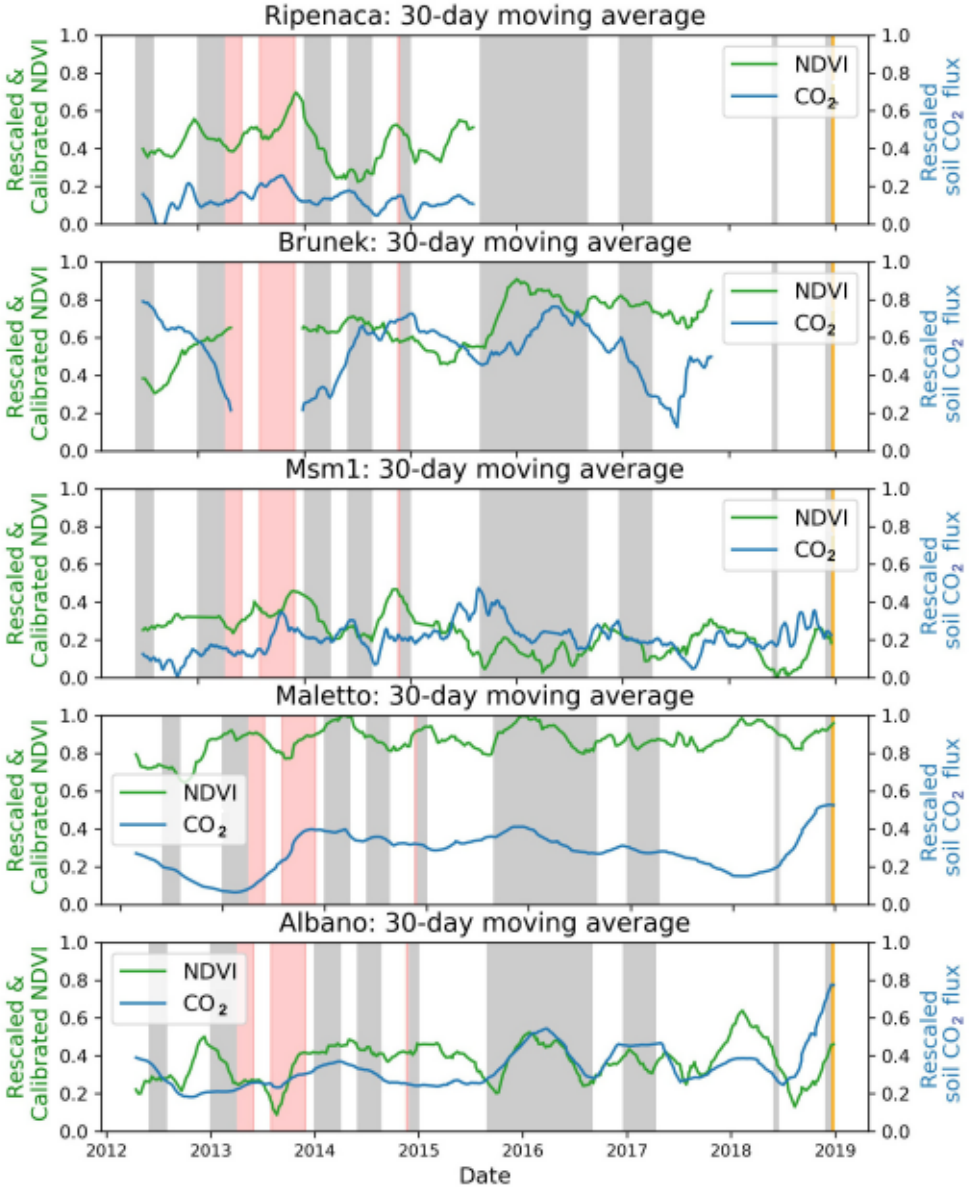

Fig. 2. Calibrated NDVI and soil CO_2 flux for Ripenaca, Brunek, Msm1, Maletto, and Albano EtnaGas stations. All signals have been rescaled and smoothed with a 30-day moving average filter. The vertical bars represent eruptive activity where the gray bars indicate strombolian activity, red bars indicate lava fountaining, and the orange bar indicates a flank eruption. The Brunek EtnaGas station is missing data from April 2013 to December 2013. (For interpretation of the references to colour in this figure legend, the reader is referred to the web version of this article.)

NDVI and soil CO_2 flux signals were rescaled to their corresponding minimum and maximum values. The buffer around the Maletto EtnaGas station had a maximum NDVI of 0.81, and the buffer nearby the Msm1 EtnaGas station had a minimum NDVI of 0.60. Keeping in mind, a limitation of NDVI >0.4 was applied during the GEE NDVI collection to remove affects from snow cover, deciduous abscission, and clouds missed in the GEE algorithm. The Brunek EtnaGas station measured the maximum soil CO_2 flux at about 0.53 $\frac{kg}{m^2 d}$ and many EtnaGas stations measured 0 $\frac{kg}{m^2 d}$ as the minimum. A 30-day moving average smoothed the rescaled signals for both calibrated NDVI and soil CO_2 flux (Fig. 2). Ripenaca and Brunek EtnaGas stations both have shortened datasets: the former was stolen in August 2015, the latter due to maintenance issues. Eruptive activity for the 2011–2018 time period is split into strombolian activity, lava fountaining, and flank eruptions, which was reviewed by Giuffrida et al. (2023) and summarized by the Global Volcanism Program (GVP; https://volcano.si.edu/volcano.cfm?vn=211060). It was expected that the soil CO_2 flux signals of the 5 stations vary in pattern and magnitude since each station measures at a different location on the Mt. Etna flank, overlying different tectonic systems and geologic features, as also seen in Liuzzo et al. (2013). Additionally, the Brunek EtnaGas station, which is positioned the closest to the most active fault system, has the overall largest magnitude soil CO_2 flux values. Furthermore, there are some visual similarities in signal pattern between each station's soil CO_2 flux and NDVI. Specifically, the increase and decrease sequences seem to correspond in time (Fig. 2). Photosynthetic activity of plants exposed to CO_2 emissions and sunlight typically have a time lag of 1–2 h (Juric et al., 1984). Liuzzo et al. (2013) modeled two end member scenarios of Mt. Etna degassing showing a systematic increase/decrease cycle of soil CO_2 flux. One end member entails the rise of magma from depth towards an intermediate storage chamber, initiating the exsolution of CO_2 volatiles which are diffusely released on the lower flanks of Mt. Etna. The EtnaGas stations measure this as a relative increase in soil CO_2 flux. The magma continues to rise towards shallow magma chambers and sometimes erupts onto the surface. This results in a relative decrease of soil CO_2 flux measured by the EtnaGas stations since most of the CO_2 has been exsolved and diffusely released at this point. The other end member involves stationary magma at depth where

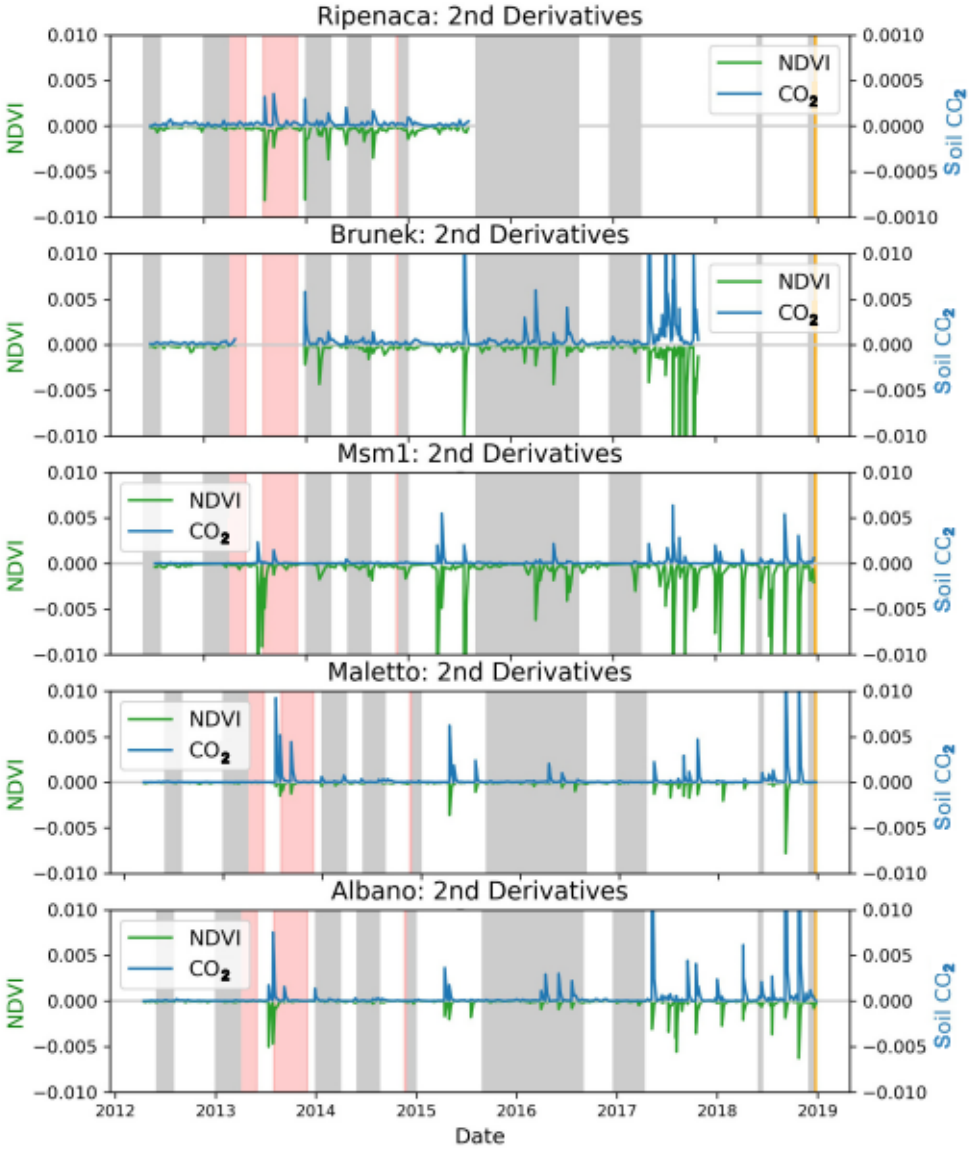

Fig. 3. 2nd derivatives of the calibrated NDVI and soil CO_2 flux for the EtnaGas stations. The vertical bars represent eruptive activity where the gray bars indicate strombolian activity, red bars indicate lava fountaining, and the orange bar indicates a flank eruption. The Brunek EtnaGas station is missing data from April 2013 to December 2013. (For interpretation of the references to colour in this figure legend, the reader is referred to the web version of this article.)

CO_2 degases until there are minimal CO_2 volatiles left, resulting in the increase/decrease shape of soil CO_2 flux at the EtnaGas stations (Liuzzo et al., 2013). These increase/decrease cycles were confirmed in a study from 2004 to 2012 on Mt. Etna, which correlated the cycles to volcanic activity at the summit craters (Liuzzo et al., 2013), as well as in subsequent eruptions (Gurrieri et al., 2021; Paonita et al., 2021). In this present study, these same increase/decrease cycles appear in both calibrated NDVI and soil CO_2 flux signals at all stations (Fig. 2).

Taking into account the positive relationship between CO_2 flux and NDVI, an assessment of the consistency of the two signals was conducted in relation to the rate of change of their respective magnitudes. To achieve this objective, we calculated the second derivative to analyze the fluctuations in the rate of change of soil CO_2 flux and NDVI over time (Appendix 1). Specifically, we aimed to determine degassing acceleration as a proxy for volcanic input and evaluate its potential impact on vegetation by examining the correlation with NDVI. The soil CO_2 flux signal was resampled to match the temporal resolution of the calibrated NDVI signal before calculating the 2nd derivative, which was 7 ± 3 days. For better graphic comparison, all 2nd derivatives for calibrated NDVI were negated and the absolute value was taken for all 2nd derivatives of soil CO_2 flux in order to have a reflection of signals on the x-axis (Fig. 3). In all cases, low magnitude 2nd derivatives of soil CO_2 are reflected by low magnitude 2nd derivatives of NDVI, and every time there is a large spike in the soil CO_2 2nd derivative, there is one for NDVI at the same time. Spikes in the 2nd derivative indicate rapid changes in the rate of change such as sudden escalations or de-escalations.

Starting in 2017, both NDVI and soil CO_2 2nd derivatives have large and more frequent fluctuations (Fig. 4). Ripenaca and Brunek EtnaGas stations are not considered because they have no and partial data covering this time period, respectively. Larger 2nd derivative spikes indicate a sharp inflection point in the change from increasing to decreasing trend for the calibrated NDVI and soil CO_2 flux. As for volcanic activity, the 2017–2018 period is described by mostly quiescent periods with minor effusive activity including a 3-day flank eruption at the end of December 2018 (Gurrieri et al., 2021; Giuffrida et al., 2023). A comprehensive analysis of soil CO_2 degassing from the EtnaGas stations, volcanic activity, and seismic activity can be found in Gurrieri et al. (2021); this more detailed activity is displayed in Fig. 4. It is important to note that during this period of quiescence, the Etnean plumbing system underwent an extended phase of extraordinary pressurization in its deepest regions (Gurrieri et al., 2021; Paonita et al., 2021). This resulted in a short-duration flank eruption, which had a significant impact on surface fracturing. Additionally, the event was accompanied by a period of heightened seismic activity, culminating in

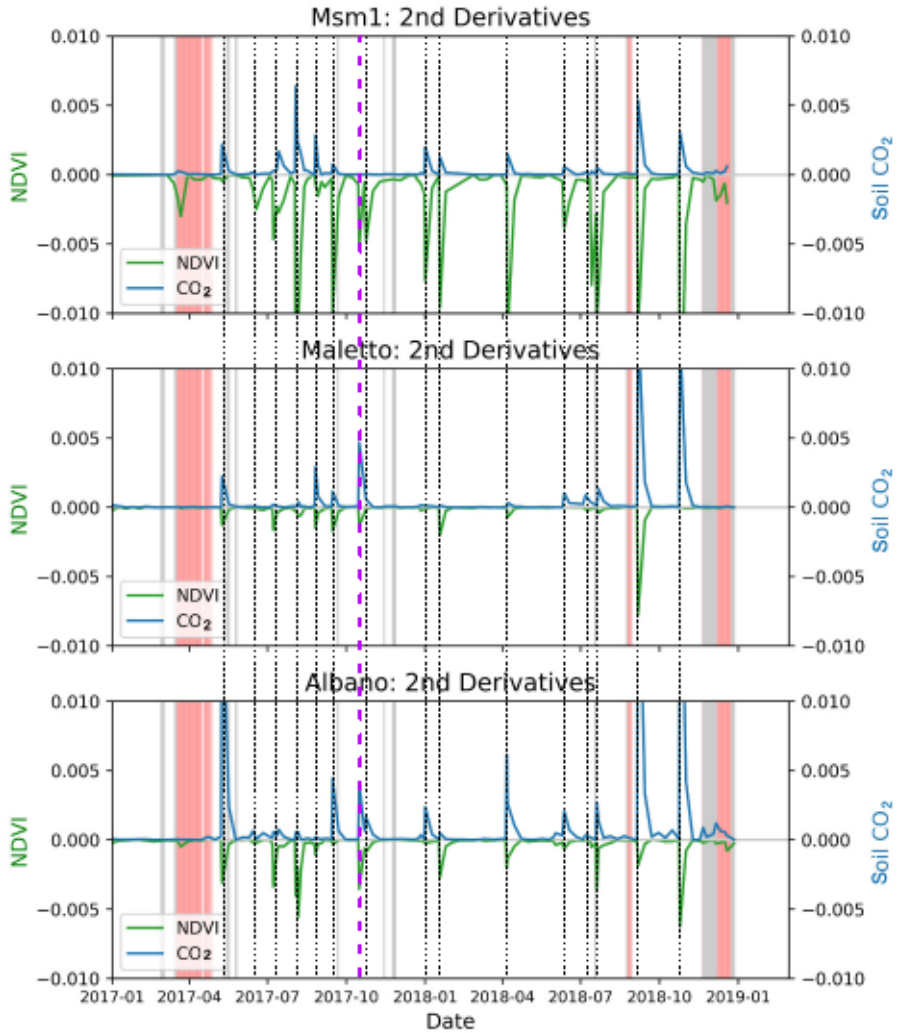

Fig. 4. 2nd derivatives of calibrated NDVI and soil CO_2 flux post 2017 for 3 EtnaGas stations. The red vertical bars represent effusive eruptive activity such as lava flows and fountains where the gray bars indicate explosive activity such as ash activity (Gurrieri et al., 2021). The dashed vertical lines correspond to concurrent spikes of soil CO_2 and NDVI across all 3 graphs. The dashed, thicker, purple line is the 10-16-2017 example. (For interpretation of the references to colour in this figure legend, the reader is referred to the web version of this article.)

the M_w 4.9 earthquake that occurred on 26 December 2018. This earthquake was the most powerful earthquake that occurred in the Etna area in over 30 years (Civico et al., 2019; Büyükakpınar et al., 2022).

Within this shortened timeline, Fig. 4 shows that with every soil CO_2 2nd derivative spike, there is a corresponding 2nd derivative NDVI spike at generally the same time and duration. The peak finder function in the SciPy library found 16 simultaneously occurring spikes in the soil CO_2 and NDVI 2nd derivatives for the Albano, Msm1, and Maletto EtnaGas stations within 0.3 3 days of each other (Fig. 4, Table 5). Any differences of spike dates across stations are likely a product of the smoothing and linear interpolation to common timeframes between the NDVI and soil CO_2 flux signals. While Albano and Msm1 EtnaGas stations have the same number and dates of spikes, Maletto is missing 3 spikes in both the CO_2 and NDVI 2nd derivative signals, likely reflecting the heterogeneity of various subsurface degassing pathways. Additionally, there are a few instances where the soil CO_2 2nd derivative shows no spike for one EtnaGas station but does for the other 2 EtnaGas stations. For example, on 10-16-2017, soil CO_2 spiked at Albano and Maletto EtnaGas stations, but not at the Msm1 EtnaGas station (Fig. 4, Table 5). However, there is a clear spike in the NDVI 2nd derivative on this day at the Msm1 EtnaGas station of intermediate magnitude (Fig. 4). This scenario is applicable for the other 3 instances when all stations do not have concurrent soil CO_2 spikes (06-18-2017, 10-24-2017, and 01-18-2018). There is never an instance when NDVI spikes without a simultaneous CO_2 spike in one or more of the EtnaGas stations, although the station is not always co-located with the NDVI spike. This implies that the 2nd derivative of NDVI might not always persistently reflect localized changes in diffuse CO_2 degassing, and the degassing activity as a whole might still influence NDVI independent of the specific site where the CO_2 station is located.

Previous studies using petrologic, thermodynamic, and geophysical research indicate that the quiescent periods of 2017 2018 are characterized by deep magmatic recharging events (Viccaro et al., 2016, 2019; Cannata et al., 2018; Borzi et al., 2020; Giuffrida et al., 2021; Giuffrida et al., 2023). Volatile-rich magma begins to rise from a deep source to the intermediate magma chambers between 2 and 6 km below sea level (Giuffrida et al., 2023). The magma continues to rise and is injected into shallow magma chambers, occasionally reaching the surface as strombolian activity or flank eruption (Giuffrida et al., 2023). These recharging events occur repeatedly throughout 2017 2018 and complement the first degassing end member scenario proposed by Liuzzo et al. (2013). The 2nd derivative graphs of multiple stations on the flanks of Mt. Etna illustrate the timeline of these 16 recharging events in both the soil CO_2 and NDVI signals. In other words, the spikes in the 2nd derivative identify the times of the switch from increasing to decreasing trends in the soil CO_2 flux measured by the EtnaGas stations on the surface; and therefore, the spikes also indicate the general timeframe when magma is ascending from an intermediate to shallow magma chamber. The soil CO_2 flux and NDVI 2nd derivative spikes are a surficial reflection of subsurface processes.

Table 5
Dates of soil CO_2 2nd derivative spikes in Fig. 4. Asterisk denotes when a soil CO_2 2nd derivative spike did not exist for that individual station, but an NDVI spike was present. Blank boxes indicate that no soil CO_2 or NDVI spike was present.

No.	Date of Spike		
	Msm1	Maletto	Albano
1	05-09-2017	05-09-2017	05-09-2017
2	*06-18-2017		06-18-2017
3	07-14-2017	07-08-2017	07-08-2017
4	08-06-2017	08-06-2017	08-06-2017
5	08-26-2017	08-26-2017	*08-26-2017
6	09-15-2017	09-15-2017	09-15-2017
7	*10-16-2017	10-16-2017	10-16-2017
8	*10-24-2017		10-24-2017
9	01 01 2018		01 01 2018
10	01-18-2018	*01-18-2018	01-18-2018
11	04-07-2018	04-07-2018	04-06-2018
12	06 12 2018	06 12 2018	06 12 2018
13	07-14-2018	07-07-2018	07-07-2018
14	07-20-2018	07 22 2018	07-20-2018
15	09-06-2018	09-06-2018	09-06-2018
16	10-25-2018	10-25-2018	10-25-2018

3.2. Flank distribution

The differences in magnitude of the soil CO_2 flux signal of each EtnaGas station and differences in 2nd derivative spikes highlights that the underlying tectonic setting, geologic features, and magma storage depth play a role in the amount of degassing that makes it to the surface. According to the 2nd derivatives, changes in the storage level of subsurface magma and subsequent release of volcanic CO_2 affect the NDVI of overlying trees on the surface. To understand how localized the effects are, the NDVI was collected and averaged for homogenous forests on the high flanks of Mt. Etna (Fig. 1a). If forests were at a lower elevation than the EtnaGas stations, it was further validated to make sure no roads, neighborhoods, buildings, or agriculture were nearby. Both Landsat 8 and Sentinel 2 NDVI were calibrated with respect to VIIRS using 2nd order polynomials and an ANOVA analysis confirmed statistically the same means (Table 6). The temperature, pressure, humidity, and active rainfall were averaged using Maletto, Msm1, and Albano EtnaGas station s environmental parameters for the regression analysis since they covered the same time of observation between 2011 and 2018. Only temperature had a moderate influence on the NDVI of Mt. Etna flank trees at r^2 0.5 and was removed.

To reduce the effects from these 3 EtnaGas stations local topography variations, different elevations, and various subsurface features that influence degassing, the signals were rescaled to create a representative soil CO_2 signal that will be hereby referenced as the flank soil CO_2 signal (Liuzzo et al., 2013; Gurrieri et al., 2021). The flank signal was calculated using the equation from Liuzzo et al. (2013):

$$\underset{Norm}{\overset{n}{}} t \qquad \overset{n}{i} \; 1 \; \frac{i \; t \qquad \overset{min}{i}}{\underset{i}{max} \qquad \underset{i}{min}} \tag{3}$$

where is the flux, i is the station, and t is the time. In other words, for each day, the rescaled flux of each station is added together (Fig. 5a; Appendix 4). The 2nd derivatives of this flank soil CO_2 signal calculated by Eq. (3) were compared with the 2nd derivatives of the flank NDVI (Fig. 5b). The 2nd derivative flank CO_2 signal shows the same spikes at the same time as the individual EtnaGas stations from 2017 to 2018 (Fig. 5b). Even with the extended dataset, when the 2nd derivative of CO_2 spikes, so does the NDVI 2nd derivative, and there is no instance when one signal doesn t spike without the other. The peak finder function in SciPy identified 28 concurrent CO_2 spikes and NDVI spikes throughout 2011 2018 (Fig. 5b). There were 2 additional NDVI spikes without concurrent CO_2 spikes between 2014 and 2015 of small magnitude that were only identified by increasing the sensitivity value in the peak finder function. A regression analysis between the 2nd derivatives of flank CO_2 and NDVI indicate a strong linear correlation (Fig. 6). The similarities between the flank and individual EtnaGas stations suggests that the 2nd derivative of all homogenous trees not near human influences reflect overall changes in the diffuse CO_2 degassing system in the Mt. Etna subsurface, indicating that it may not be necessary to have localized collection buffers for NDVI along volcano-tectonic structures.

Table 6
NDVI calibration equations for the flank of Mt. Etna.

	2nd order polynomials							
	Landsat 8 NDVI w.r.t. VIIRS				Sentinel 2 NDVI w.r.t. VIIRS			
Flank	y	2.26	^{2} 3.04	0.93	y	0.87	^{2} 0.89	0.22

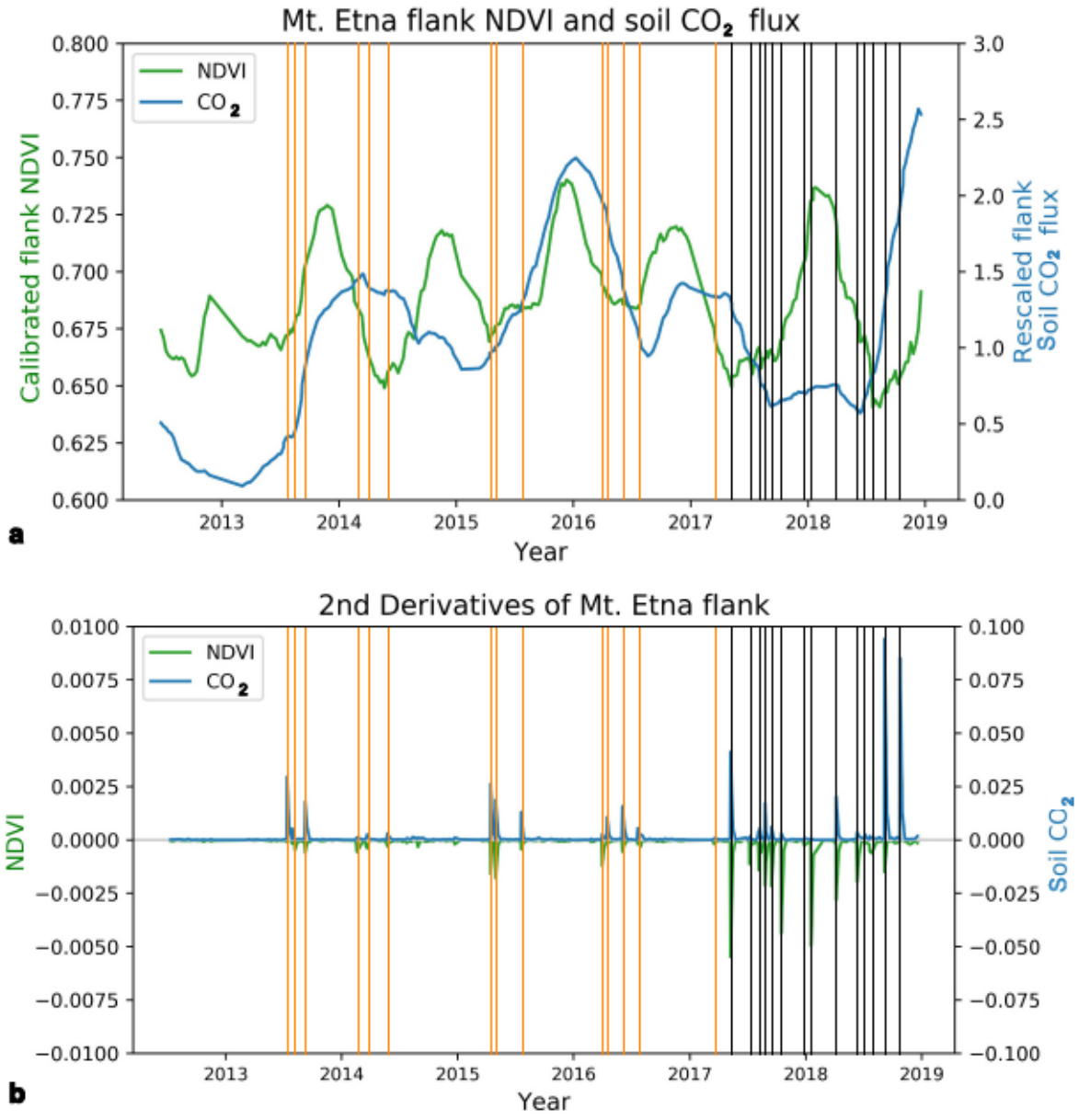

Fig. 5. a. Calibrated NDVI values from all the trees on the upper flanks of Mt. Etna from Fig. 1a in green and the rescaled flank soil CO_2 flux calculated by Eq. (3) from Maletto, Msm1, and Albano EtnaGas stations in blue. The thin, gray lines represent the same spike as Fig. 4 and Table 5. The thin, orange lines indicate the additional spikes of CO_2 and NDVI 2nd derivatives from Fig. 5b. The 2nd derivative spikes occasionally do not line up with peaks in the calibrated NDVI and rescaled flank soil CO_2 flux due to the concentration of data points (Appendix 1). 7b) Negated 2nd derivatives of the flank NDVI signal from Fig. 5a in green and the 2nd derivative absolute values of the flank soil CO_2 flux from Fig. 5a in blue. The thin, gray lines represent the same spike as Fig. 4 and Table 5. The thin, orange lines indicate the additional spikes of CO_2 and NDVI 2nd derivatives. (For interpretation of the references to colour in this figure legend, the reader is referred to the web version of this article.)

4. Application

NDVI can be collected all over the world with a variety of airborne and spaceborne sensors and satellites in the absence of clouds cover, highlighting the ease of remote data collection and temporal frequency. Mt. Etna is one of the only volcanoes in the world with several continuous soil CO_2 flux sensors on its flanks and enough data to characterize the behavior of CO_2 degassing with volcanic activity. Diffuse CO_2 degassing is inadequately measured for many volcanic systems, but assessing the NDVI signals of vegetation on volcanoes can fill in some of the gaps once the relationship between CO_2 emissions and vegetation health for different species and growing seasons is understood.

When applying the 2nd derivative NDVI method to other vegetated volcanoes, many factors need to be considered. It is important that trees are not close to human influences like agriculture and neighborhoods. If multiple sensors are used to calculate NDVI, an intercalibration technique will need to be applied to normalize NDVI across sensors. While temperature was the main environmental parameter affecting NDVI on Mt. Etna, this may not be the case on other volcanoes with different ecosystems. Other environmental factors like atmospheric pressure, precipitation, and other stressors can have effects on trees. Additionally, the NDVI collections on Mt. Etna only used deciduous and coniferous trees. More research needs to be done on tropical trees and how they react to volcanic CO_2. Past isotopic studies have shown that tropical plants incorporate volcanic CO_2 into their photosynthesis processes (Bogue et al., 2019), indicating the potential that tropical systems may

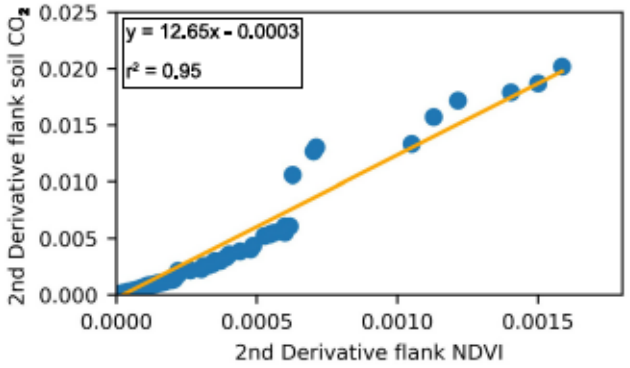

Fig. 6. There is a strong linear correlation between the absolute value 2nd derivatives of flank NDVI and soil CO_2 from Fig. 5b. The outliers (3σ) were removed from both signals before calculating the correlation. The best fit line equation and r^2 is shown in the box.

react in a similar fashion for NDVI. Future FACE experiments in the Amazon will reduce uncertainties of tropical plant ecosystem response to projected, atmospheric CO_2 levels (Hofhansl et al., 2016). Furthermore, groups of trees over at least several pixels depending on the spatial resolution of the imagery should be used when averaging NDVI and applying a filter of NDVI >0.4 to remove snow, clouds, and deciduous abscission outliers. The groups of trees should be homogenous, without large spaces for bare ground or grass that would artificially lower the NDVI. Using large polygons to average NDVI highlights the applicability of low spatial resolution imagery like MODIS and VIIRS to conduct the NDVI timeseries assessment.

Just as different ecosystems are variably influenced by external parameters, each volcanic system also varies. Mt. Etna is likely an end member situation since the trees reflected the same 2nd derivative pattern on the upper flanks no matter the proximity to volcano-tectonic structures. Further comparative studies are needed in volcanic systems beyond Etna to better understand the potential differences in the impacts of emissions on vegetative areas. It is likely that the extent and magnitude of CO_2 outgassing, as well as the presence of other gaseous species such as hydrogen halides, fluorides, SO_2, and H_2S, could have a significant influence on the NDVI in areas with significant degassing of geothermal origin (Wardell et al., 2004; Nelson and Sewake, 2008; D'Arcy et al., 2019; Linhares et al., 2019; Cadoux et al., 2022; Bogue et al., 2023). H_2S is a commonly released volatile and impairs root growth in plants (Nelson and Sewake, 2008). Hydrogen halides and SO_2 easily dissolve in water and can produce acid rain, causing leaf impairment (D'Arcy et al., 2019; Cadoux et al., 2022). A high concentration of fluorides can cause necrosis and leaf loss (Linhares et al., 2019). However, most of these gases generally have a localized impact near hydro/geo-thermal areas or near the volcano crater vent, whereas CO_2 is widespread on all sides of volcanic areas and has the potential to affect enormously large areas. These gases are not typically present in volcanic contexts such as Etna, and their impact on vegetation should be explored in different types of volcanic systems. For example, plants exposed to ash emissions downwind of the plume of Turrialba Volcano, Costa Rica, were affected by volcanic SO_2 and CO_2, stressing the need to take into account all gaseous species (D'Arcy et al., 2019). As an opposite end member, the tree kill areas in Yellowstone are spatially constrained by the surficial expressions of faults and fractures. The volcano-tectonic structures control the movement of fluids from the source to be released in concentrated amounts at the surface (Vaughan et al., 2020). Particularly, inside the Tern Lake thermal area, the tree kill zones had anomalous NDVI signals when compared to trees outside the thermal area, indicating beneficial influence from diffuse volcanic volatiles before death (Bogue et al., 2023). While the volcano-tectonic setting was not needed to understand the NDVI signal on Mt. Etna, it will be crucial for other systems especially with a strong hydro/geothermal activity component.

5. Conclusion

The soil CO_2 flux of 5 EtnaGas stations and co-located NDVI signals of nearby trees were compared to assess any correlation. The NDVI and soil CO_2 flux signals show repeating increase/decrease cycles, or pulses of diffusely degassed, volcanic CO_2 releasing at the surface depending on changes in the magma storage levels. The 2nd derivative spikes of both NDVI and soil CO_2 flux in 3 EtnaGas stations distinguish 16 magma recharge events from 2017 to 2018. The 2nd derivative spikes can be used as a timestamp for changing magmatic storage levels. An entire flank analysis of homogenous trees across Mt. Etna showed the same 2nd derivative spike pattern for NDVI, indicating that trees do not have to be located near volcano-tectonic structures to be affected by diffusely escaping volcanic CO_2. This NDVI method has the potential to be applied to other vegetated volcanoes that lack intensive CO_2 monitoring considering tree type, environmental parameters, and typical volcanic system behavior. The effectiveness of this technique is particularly noteworthy when applied in volcanic regions where ground-based monitoring systems for CO_2 emissions are challenging to implement, such as economically disadvantaged countries or those with political or social obstacles that impede the establishment of a comprehensive monitoring network. Additionally, the capacity to remotely monitor volcanic CO_2 emissions eliminates the logistics and risks associated with accessing and maintaining instruments in volcanic areas that are difficult to reach but pose significant risks to people living in their vicinity, such as some volcanoes in Central America or Africa. This study is the first of its kind to show an in-depth correlation between the NDVI of trees, volcanic CO_2, and magmatic activity.

CRediT authorship contribution statement

Nicole K. Guinn: Writing – original draft, Visualization, Validation, Software, Project administration, Methodology, Investigation, Formal analysis, Data curation, Conceptualization. **Craig Glennie:** Writing – review & editing, Supervision, Methodology, Funding acquisition, Conceptualization. **Marco Liuzzo:** Writing – review & editing, Resources, Data curation, Conceptualization. **Giovanni Giuffrida:** Writing – review & editing. **Sergio Gurrieri:** Writing – review & editing.

Declaration of competing interest

The authors declare that they have no known competing financial interests or personal relationships that could have appeared to influence the work reported in this paper.

Data availability

Data will be made available on request.

Acknowledgements

The authors would like to thank Jennifer Lewicki, U.S. Geological Survey, for her input on proposals and abstract submissions for conferences describing early progress on this work. Also, thanks to Francisco Haces-Garcia at the National Center for Airborne Laser Mapping for coding assistance. Partial funding for the first and second authors was provided by a facility grant from the National Science Foundation (#1830734) and the U.S. Army Corps of Engineers Cold Regions Research and Engineering Laboratory (USACE-CRREL).

Appendix A. Supplementary data

Supplementary data to this article can be found online at https://doi.org/10.1016/j.rse.2024.114408.

References

Acocella, V., Ripepe, M., Rivalta, E., Peltier, A., Galetto, F., Joseph, E., 2023. Towards scientific forecasting of magmatic eruptions. Nat. Rev. Earth Environ. 5 (1), 5 22. https://doi.org/10.1038/s43017-023-00492-z.

Ainsworth, E.A., Long, S.P., 2005. What have we learned from 15 years of free-air CO_2 enrichment (FACE)? A meta-analytic review of the responses of photosynthesis, canopy properties and plant production to rising CO_2. New Phytol. 165 (2), 351 372. https://doi.org/10.1111/j.1469-8137.2004.01224.x.

Aiuppa, A., Moretti, R., Federico, C., Giudice, G., Gurrieri, S., Liuzzo, M., Papale, P., Shinohara, H., Valenza, M., 2007. Forecasting Etna eruptions by real-time observation of volcanic gas composition. Geol 35 (12), 1115 1118. https://doi.org/10.1130/G24149A.1.

Aiuppa, A., Fischer, T.P., Plank, T., Bani, P., 2019. CO_2 Flux Emissions from the Earth s Most Actively Degassing Volcanoes, 2005-2015, 9, p. 5442. https://doi.org/10.1038/s41598-019-41901-y.

Allard, P., Carbonnelle, J., Dajlevic, D., Le Bronec, J., Morel, P., Robe, M.C., Maurenas, J. M., Faivre-Pierret, R., Martin, D., Sabroux, J.C., Zettwoog, P., 1991. Eruptive and diffuse emissions of CO_2 from Mount Etna. Nature 351 (6325), 387 391. https://doi.org/10.1038/351387a0.

Allard, P., Behncke, B., D Amico, S., Neri, M., Gambino, S., 2006. Mount Etna 1993-2005: anatomy of an evolving eruptive cycle. Earth Sci. Rev. 78 (1 2), 85 114. https://doi.org/10.1016/j.earscirev.2006.04.002.

Barreca, G., Bonforte, A., Neri, M., 2013. A pilot GIS database of active faults of Mt. Etna (Sicily): a tool for integrated hazard evaluation. J. Volcanol. Geotherm. Res. 251, 170 186. https://doi.org/10.1016/j.jvolgeores.2012.08.013.

Behncke, B., Neri, M., 2003. Cycles and trends in the recent eruptive behaviour of Mount Etna (Italy). Can. J. Earth Sci. 40 (10), 1405 1411. https://doi.org/10.1139/e03-052.

Bogue, R.R., Schwandner, F.M., Fisher, J.B., Pavlick, R., Magney, T.S., Famiglietti, C.A., Cawse-Nicholson, K., Yadav, V., Linick, J.P., North, G.B., Duarte, E., 2019. Plant responses to volcanically elevated CO_2 in two Costa Rican forests. Biogeosciences 16 (6), 1343 1360. https://doi.org/10.5194/bg-16-1343-2019.

Bogue, R.R., Douglas, P.M.J., Fisher, J.B., Stix, J., 2023. Volcanic diffuse volatile emissions tracked by plant responses detectable from space. Geochem. Geophys. 24 (11), e2023GC010938 https://doi.org/10.1029/2023GC010938.

Bonaccorso, A., Bonforte, A., Calvari, S., Del Negro, C., Di Grazia, G., Ganci, G., Neri, M., Vicari, A., Boschi, E., 2011. The initial phases of the 2008-2009 Mount Etna eruption: a multidisciplinary approach for hazard assessment. J. Geophys. Res. Solid Earth 116 (3), 1 19. https://doi.org/10.1029/2010JB007906.

Borzi, A.M., Giuffrida, M., Zuccarello, F., Palano, M., Viccaro, M., 2020. The Christmas 2018 eruption at Mount Etna: enlightening how the volcano factory works through a multiparametric inspection. Geochem. Geophys. 21 (10), 1 15. https://doi.org/10.1029/2020GC009226.

Bottinga, Y., Javoy, M., 1990. MORB degassing: bubble growth and ascent. Chem. Geol. 81 (4), 255 270. https://doi.org/10.1016/0009-2541(90)90050-H.

Brantley, S.L., Koepenick, K.W., 1995. Measured carbon dioxide emissions from Oldoinyo Lengai and the skewed distribution of passive volcanic fluxes. Geol 23 (10), 933 936. https://doi.org/10.1130/0091-7613(1995)023 0933:MCDEFO 2.3.CO;2.

Burton, M.R., Oppenheimer, O., Horrocks, L.A., Francis, P.W., 2000. Remote sensing of CO_2 and H_2O emission rates from Masaya volcano, Nicaragua. Geol 28 (10), 915 918. https://doi.org/10.1130/0091-7613(2000)28 915:RSOCAH 2.0.CO;2.

Burton, M.R., Neri, M., Andronico, D., Branca, S., Caltabiano, T., Calvari, S., Corsaro, R. A., Del Carlo, P., Lanzafame, G., Lodato, L., Miraglia, L., Salerno, G., Spampinato, L., 2005. Etna 2004-2005: an archetype for geodynamically-controlled effusive eruptions. Geophys. Res. Lett. 32 (9), 1 4. https://doi.org/10.1029/2005GL022527.

Burton, M.R., Sawyer, G.M., Granieri, D., 2013. Deep carbon emissions from volcanoes. RiMG v75, 323 354. https://doi.org/10.2138/rmg.2013.75.11.

Büyükakpınar, P., Cannata, A., Cannavo, F., Carbone, D., De Plaen, R.S.M., Di Grazia, G., King, T., Lecocq, T., Liuzzo, M., Salerno, G., 2022. Chronicle of processes leading to the 2018 eruption at Mt. Etna as inferred by seismic ambient noise along with geophysical and geochemical observables. J. Geophys. Res. Solid Earth 127, e2022JB025024. https://doi.org/10.1029/2022JB025024.

Cadoux, A., Tegtmeier, S., Aiuppa, A., 2022. Natural halogen emissions to the Atmopshere: sources, flux, and environmental impact. Elements 18 (1), 27 33. https://doi.org/10.2138/gselements.18.1.27.

Camarda, M., Gurrieri, S., Valenza, M., 2006a. CO_2 flux measurements in volcanic areas using the dynamic concentration method: influence of soil permeability. J. Geophys. Res. Solid Earth 111 (5), 1 14. https://doi.org/10.1029/2005JB003898.

Camarda, M., Gurrieri, S., Valenza, M., 2006b. In situ permeability measurements based on a radial gas advection model: relationships between soil permeability and diffuse CO_2 degassing in volcanic areas. Pure Appl. Geophys. 163 (4), 897 914. https://doi.org/10.1007/s00024-006-0045-y.

Cannata, A., Di Grazia, G., Giuffrida, M., Gresta, S., Palano, M., Sciotto, M., Viccaro, M., Zuccarello, F., 2018. Space-time evolution of magma storage and transfer at Mt. Etna volcano (Italy): the 2015 2016 reawakening of Voragine crater. Geochem. Geophys. 19 (2), 471 495. https://doi.org/10.1002/2017GC007296.

Cawse-Nicholson, K., Fisher, J.B., Famiglietti, C., Braverman, A., Schwandner, F.M., Lewicki, J.L., Townsend, P.A., Schimel, D.S., Pavlick, R., Bormann, K.J., Ferraz, A., Kang, E.L., Ma, P., Bogue, R.R., Youmans, T., Pieri, D.C., 2018. Ecosystem responses to elevated CO_2 using airborne remote sensing at Mammoth Mountain, California. Biogeosciences 15 (24), 7403 7418. https://doi.org/10.5194/bg-15-7403-2018.

Chiodini, G., Cioni, R., Guidi, M., Raco, B., Marini, L., 1998. Soil CO_2 flux measurements in volcanic and geothermal areas. J. Appl. Geochem. 13 (5), 543 552. https://doi.org/10.1016/S0883-2927(97)00076-0.

Civico, R., Pucci, S., Nappi, R., Azzaro, R., Villani, F., Pantosti, D., et al., 2019. Surface ruptures following the 26 December 2018, Mw 4.9, Mt. Etna earthquake, Sicily (Italy). J. Maps. 15 (2), 831 837. https://doi.org/10.1080/17445647.2019.1683476.

Cook, A.C., Hainsworth, L.J., Sorey, M.L., Evans, W.C., Southon, J.R., 2001. Radiocarbon studies of plant leaves and rings from mammoth mountain, CA: a long-term record of magmatic CO_2 release. Chem. Geol. 177 (1 2), 117 131. https://doi.org/10.1016/S0009-2541(00)00386-7.

Curtis, P.S., Wang, X., 1998. A meta-analysis of elevated CO_2 effects on woody plant mass, form, and physiology. Oecologia 113 (3), 299 313. https://doi.org/10.1007/s004420050381.

D Arcy, F., Boucher, E., Maarten De Moor, J., Helie, J.-F., Piggott, R., Stix, J., 2019. Carbon and sulfur isotopes in tree rings as a proxy for volcanic degassing. Geology 47 (9), 825 828. https://doi.org/10.1130/G46323.1.

De Gregorio, S., Diliberto, I.S., Giammanco, S., Gurrieri, S., Valenza, M., 2002. Tectonic control over large-scale diffuse degassing in eastern Sicily (Italy). Geofluids 2, 273 284. https://doi.org/10.1046/j.1468-8123.2002.00043.x.

Dietrich, R., Bell, F.W., Silva, L.C.R., Cecile, A., Horwath, W.R., Anand, M., 2016. Climatic sensitivity, water-use efficiency, and growth decline in boreal jack pine (Pinus banksiana) forests in northern Ontario. Biogeosciences 121 (10), 2761 2774. https://doi.org/10.1002/2016JG003440.

Drake, B.G., Gonzalez-Meler, M.A., Long, S.P., 1997. More efficient plants: a consequence of rising atmospheric CO_2? Annu. Rev. Plant Biol. 48, 609 639. https://doi.org/10.1146/annurev.arplant.48.1.609.

Evans, W.C., Bergfeld, D., McGeehin, J.P., King, J.C., Heasler, H., 2010. Tree-ring 14C links seismic swarm to CO_2 spike at Yellowstone, USA. Geol 38 (12), 1075 1078. https://doi.org/10.1130/G31345.1.

Farrar, C.D., Sorey, M.L., Evans, W.C., Howle, J.F., Kerr, B.D., Kennedy, B.M., King, C.Y., Southon, J.R., 1995. Forest-killing diffuse CO_2 emission at mammoth mountain as a sign of magmatic unrest. Nature 376 (6542), 675 678. https://doi.org/10.1038/376675a0.

Fernandez, M.D., Pieters, A., Donoso, C., Tezara, W., Azkue, M., Herrera, C., Rengifo, E., Herrera, A., 1998. Effects of a natural source of very high CO_2 concentration on the leaf gas exchange, xylem water potential and stomatal characteristics of plants of Spatiphylum cannifolium and Bauhinia multinervia. New Phytol. 138 (4), 689 697. https://doi.org/10.1046/j.1469-8137.1998.00161.x.

Gardner, J.E., Hilton, M., Carroll, M.R., 2000. Bubble growth in highly viscous silicate melts during continuous decompression from high pressure. Geochim. Cosmochim. Acta 64 (8), 1473 1483. https://doi.org/10.1016/S0016-7037(99)00436-6.

Giuffrida, M., Scandura, M., Costa, G., Zuccarello, F., Sciotto, M., Cannata, A., Viccaro, M., 2021. Tracking the summit activity of Mt. Etna volcano between July 2019 and January 2020 by integrating petrological and geophysical data. J. Volcanol. Geotherm. Res. 418, 107350 https://doi.org/10.1016/j.jvolgeores.2021.107350.

Giuffrida, M., Cardone, M., Zuccarello, F., Viccaro, M., 2023. Earth-Science Reviews Etna 2011 2022: Discoveries from a decade of activity at the volcano. Earth Sci. Rev. 245, 104563 https://doi.org/10.1016/j.earscirev.2023.104563.

Gurrieri, S., Valenza, M., 1988. Gas transport in natural porous medium: a method for measuring soil CO_2 flows from the ground in volcanic and geothermal areas. Rend. Soc. Ital. Petrol. 43, 1151 1158.

Gurrieri, S., Liuzzo, M., Giudice, G., 2008. Continuous monitoring of soil CO_2 flux on Mt. Etna: The 2004 2005 eruption and the role of regional tectonics and volcano tectonics. J. Geophys. Res. Solid Earth 113, 1 9. https://doi.org/10.1029/2007JB005003.

Gurrieri, S., Liuzzo, M., Giuffrida, G., Boudoire, G., 2021. The first observations of CO_2 and CO_2/SO_2 degassing variations recorded at Mt. Etna during the 2018 eruptions followed by three strong earthquakes. Ital. J. Geosci. 140, 95 106. https://doi.org/10.3301/IJG.2020.25.

Hashim, H., Abd Latif, Z., Adnan, N.A., 2019. Urban vegetation classification with NDVI threshold value method with very high resolution (VHR) pleiades imagery. Int. Arch. Photogramm. Remote. Sens. Spat. Inf. Sci. XLII-4/W16, 237 240. https://doi.org/10.5194/isprs-archives-XLII-4-W16-237-2019.

Heinzel, V., Franke, J., Menz, G., 2006. Assessment of cross-sensor NDVI-variations caused by spectral band characteristics. Remote Sens. Model. Ecosyst. Sustain. III. 6298, 62980Z https://doi.org/10.1117/12.680278.

Hofhansl, F., Andersen, K.M., Fleischer, K., Fuchslueger, L., Rammig, A., Schaap, K.J., Valverde-Barrantes, O.J., Lapola, D.M., 2016. Amazon Forest ecosystem responses to elevated atmospheric CO_2 and alterations in nutrient availability: filling the gaps with model-experiment integration. Biogeoscience v4. https://doi.org/10.3389/feart.2016.00019.

Houlie, N., Komorowski, J.C., de Michele, M., Kasereka, M., Ciraba, H., 2006. Early detection of eruptive dykes revealed by normalized difference vegetation index (NDVI) on Mt. Etna and Mt. Nyiragongo. Planet. Sci. J. 246 (3 4), 231 240. https://doi.org/10.1016/j.epsl.2006.03.039.

Juric, T.W., Weber, J.A., Gates, D.M., 1984. Short-term effects of CO_2 on gas exchange of leaves of Bigtooth Aspen (*Populus grandidentata*) in the field. Plant Physiol. 75, 1022 1026. https://doi.org/10.1104/pp.75.4.1022.

Kern, C., Masias, P., Apaza, F., Reath, K.A., Platt, U., 2017. Remote measurement of high preeruptive water vapor emissions at Sabancaya volcano by passive differential optical absorption spectroscopy. J. Geophys. Res. Solid Earth 122 (5), 3540 3564. https://doi.org/10.1002/2017JB014020.

Kizilgeci, F., Yildirim, M., Islam, M.S., Ratnasekera, D., Iqbal, M.A., Sabagh, A.E.L., 2021. Normalized difference vegetation index and chlorophyll content for precision nitrogen management in durum wheat cultivars under semi-arid conditions. Sustainability 13 (7), 1 11. https://doi.org/10.3390/su13073725.

Korner, C., Asshoff, R., Bignucolo, O., Hattenschwiler, S., Keel, S.G., Pelaez-Riedl, S., Pepin, S., Siegwolf, R.T.W., Zotz, G., 2005. Ecology: carbon flux and growth in mature deciduous forest trees exposed to elevated CO_2. Science 309 (5739), 1360 1362. https://doi.org/10.1126/science.1113977.

LaDeau, S.L., Clark, J.S., 2001. Rising CO_2 levels and the fecundity of forest trees. Science 292 (5514), 95 98. https://doi.org/10.1126/science.1057547.

Laksono, A., Saputri, A.A., Izumi, B., Arkan, M.Z., Putri, R., 2020. Vegetation covers change and its impact on Barchan dune morphology in Parangtritus coast, Indonesia. In: The 1st Geosciences and Environmental Sciences Symposium, v200. https://doi.org/10.1051/e3conf/202020002026.

Lewicki, J.L., 2021. Long-term year-round observations of magmatic CO_2 emissions on Mammoth Mountain, California, USA. J. Volcanol. Geotherm. Res. 418, 107347 https://doi.org/10.1016/j.jvolgeores.2021.107347.

Lewicki, J.L., Hilley, G.E., Tosha, T., Aoyagi, R., Yamamoto, K., Benson, S.M., 2007. Dynamic coupling of volcanic CO_2 flow and wind at the horseshoe Lake tree kill, Mammoth Mountain, California. Geophys. Res. Lett. 34, L03401 https://doi.org/10.1029/2006GL028848.

Lewicki, J.L., Hilley, G.E., Shelly, D.R., King, J.C., McGeehin, J.P., Mangan, M., Evans, W. C., 2014. Crustal migration of CO_2-rich magmatic fluids recorded by tree-ring radiocarbon and seismicity at Mammoth Mountain, CA, USA. Planet. Sci. J. 390, 52 58. https://doi.org/10.1016/j.epsl.2013.12.035.

Lewicki, J.L., Kelly, P.J., Bergfeld, D., Vaughan, R.G., Lowenstern, J.B., 2017. Monitoring gas and heat emissions at Norris Geyser Basin, Yellowstone National Park, USA based on a combined eddy covariance and multi-GAS approach. J. Volcanol. Geotherm. Res. 347, 312 326. https://doi.org/10.1016/j.jvolgeores.2017.10.001.

Lewicki, J.L., Evans, W.C., Montgomery-Brown, E.K., Mangan, M.T., King, J.C., Hunt, A. G., 2019. Rate of magma supply beneath Mammoth Mountain, California, based on helium isotopes and CO_2 emissions. Geophys. Res. Lett. 46 (9), 4636 4644. https://doi.org/10.1029/2019GL082487.

Linhares, D.P.S., Garcia, P.V., Rodrigues, A.D.S., 2019. Fluoride in volcanic areas: a case study in medical geology. Environ. Health. https://doi.org/10.5772/intechopen.86058.

Liuzzo, M., Gurrieri, S., Giudice, G., Giuffrida, G., Nazionale, I., Palermo, S., 2013. Ten years of soil CO_2 continuous monitoring on Mt. Etna: exploring the relationship between processes of soil degassing and volcanic activity. Geochem. Geophys. 14 (8), 2886 2899. https://doi.org/10.1002/ggge.20196.

Liuzzo, M., Di Muro, A., Giudice, G., Michon, L., Ferrazzini, V., Gurrieri, S., 2015. New evidence of CO_2 soil degassing anomalies on piton de la Fournaise volcano and the link with volcano tectonic structures. Geochem. Geophys. 16, 4388 4404. https://doi.org/10.1002/2015GC006032.

Liuzzo, M., Di Muro, A., Rizzo, A.L., Caracausi, A., Grassa, F., Fournier, N., Shafik, B., Boudoire, G., Coltorti, M., Moreira, M., Italiano, F., 2021. Gas geochemistry at Grande Comore and Mayotte Volcanic Islands (Comoros archipelago), Indian Ocean. Geochem. Geophys. 22 (8), e2021GC009870 https://doi.org/10.1029/2021GC009870.

Marín, O., Rengifo, E., Herrera, A., Tezara, W., 2005. Seasonal changes in water relations, photosynthesis and leaf anatomy of two species growing along a natural CO_2 gradient. Interciencia 30 (1), 33 38. https://ve.scielo.org/scielo.php?script sci_arttext&pid S0378-18442005000100007.

Nelson, S., Sewake, K., 2008. Volcanic Emissions Injury Plant Foliage. UH-CTAHR. PD-47. https://citeseerx.ist.psu.edu/document?repid rep1&type pdf&doi 4e3fa4f97e34fd3be13bb1d6e3a9b34563f521de.

Nuccio, P.M., Paonita, A., 2001. Magmatic degassing of multicomponent vapors and assessment of magma depth: application to Vulcano Island (Italy). Planet. Sci. J. 193 (3 4), 467 481. https://doi.org/10.1016/S0012-821X(01)00512-X.

Paonita, A., Liuzzo, M., Salerno, G., Federico, C., Bonfanti, P., Caracausi, A., Giudice, G., 2021. Intense overpressurization at basaltic open-conduit volcanoes as inferred by geochemical signals: The case of the Mt. Etna December 2018 eruption. Sci. Adv. 7 (36) https://doi.org/10.1126/sciadv.abg6297.

Pasquier-Cardin, A., Allard, P., Ferreira, T., Hatte, C., Coutinho, R., Fontugne, M., Jaudon, M., 1999. Magma-derived CO_2 emissions recorded in 14C and 13C content of plants growing in Furnas caldera, Azores. J. Volcanol. Geotherm. Res. 92 (1 2), 195 207. https://doi.org/10.1016/S0377-0273(99)00076-1.

Proussevitch, A.A., Sahagian, D.L., 1998. Dynamics and energetics of bubble growth in magmas: analytical formulation and numerical modeling. J. Geophys. Res. Solid Earth 103 (8), 18223 18251. https://doi.org/10.1029/98jb00906.

Rahilly, K.E., Fischer, T.P., 2021. Total diffuse CO_2 flux from Yellowstone caldera incorporating high CO_2 emissions from cold degassing sites. J. Volcanol. Geotherm. Res. 419, 107383 https://doi.org/10.1016/j.jvolgeores.2021.107383.

Richardson, A.J., Wiegand, C.L., 1977. Distinguishing vegetation from soil background information. Photogramm. Eng. Remote. Sens. 43 (12), 1541 1552.

Saban, J.M., Chapman, M.A., Taylor, G., 2019. FACE facts hold for multiple generations: evidence from natural CO_2 springs. Glob. Chang. Biol. 25 (1), 1 11. https://doi.org/10.1111/gcb.14437.

Schwandner, F.M., Gunson, M.R., Miller, C.E., Carn, S.A., Eldering, A., Krings, T., Verhulst, K.R., Schimel, D.S., Hguyen, H.M., Crisp, D., O Dell, C.W., Osterman, G.B., Iraci, L.T., Podolske, J.R., 2017. Spaceborne detection of localized carbon dioxide sources. Science 358, 192. https://doi.org/10.1126/science.aam5782.

Sciandrello, S., Minissale, P., del Gado, G.G., 2020. Vascular plant species diversity of Mt. Etna (Sicily): endemicity, insularity and spatial patterns along the altitudinal gradient of the highest active volcano in Europe. PeerJ 8, e9875. https://doi.org/10.7717/peerj.9875.

Seiler, R., Kirchner, J.W., Krusic, P.J., Tognetti, R., Houlie, N., Andronico, D., Cullotta, S., Egli, M., D Arrigo, R., Cherubini, P., 2017. Insensitivity of tree-ring growth to temperature and precipitation sharpens the puzzle of enhanced pre-eruption NDVI on Mt. Etna (Italy). PLoS One 12 (1). https://doi.org/10.1371/journal.pone.0169297.

Seiler, R., Hajdas, I., Saurer, M., Houlie, N., D Arrigo, R., Kirchner, J.W., Cherubini, P., 2021. Tree-ring stable isotopes and radiocarbon reveal pre- and post-eruption effects of volcanic processes on trees on Mt. Etna (Sicily, Italy). Ecohydrology 1 15 e2340. https://doi.org/10.1002/eco.2340.

Symonds, R., 1998. Composition, Origins, Emission Rates and Atmospheric Impacts of Volcanic Gases. Open-File Report 98-776. https://doi.org/10.3133/ofr98776.

Symonds, R.B., Gerlach, T.M., Reed, M.H., 2001. Magmatic gas scrubbing: implications for volcano monitoring. J. Volcanol. Geotherm. Res. 108 (1 4), 303 341. https://doi.org/10.1016/S0377-0273(00)00292-4.

Urbazaev, M., Thiel, C., Cremer, F., Dubayah, R., Migliavacca, M., Reichstein, M., Schmullius, C., 2018. Estimation of forest aboveground biomass and uncertainties by integration of field measurements, airborne LiDAR, and SAR and optical satellite data in Mexico. Carbon Balance Manag. 13 (1) https://doi.org/10.1186/s13021-018-0093-5.

Vaughan, R.G., Hungerford, J.D.G., Keller, W., 2020. A newly emerging thermal area in Yellowstone. Front. Earth Sci. 8, 1 19. https://doi.org/10.3389/feart.2020.00204.

Viccaro, M., Giuffrida, M., Nicotra, E., Cristofolini, R., 2016. Timescales of magma storage and migration recorded by olivine crystals in basalts of the March-April 2010 eruption at Eyjafjallajökull volcano, Iceland. Am. Mineral. 101, 222 230. https://doi.org/10.2138/am-2016-5365.

Viccaro, M., Giuffrida, M., Zuccarello, F., Scandura, M., Palano, M., Gresta, S., 2019. Violent paroxysmal activity drives self-feeding magma replenishment at Mt. Etna. Sci. Rep. 9 (1), 1 15. https://doi.org/10.1038/s41598-019-43211-9.

Wardell, L.J., Kyle, P.R., Chaffin, C., 2004. Carbon dioxide and carbon monoxide emission rates from an alkaline intra-plate volcano: Mt. Erebus, Antarctica. J. Volcanol. Geotherm. Res. 131 (1 2), 109 121. https://doi.org/10.1016/S0377-0273(03)00320-2.